Bioinformatics, 31(17), 2015, 2808–2815
doi: 10.1093/bioinformatics/btv282
Advance Access Publication Date: 5 May 2015
Original Paper

OXFORD

Structural bioinformatics

Automated band annotation for RNA structure probing experiments with numerous capillary electrophoresis profiles

Seungmyung Lee[1], Hanjoo Kim[1], Siqi Tian[2], Taehoon Lee[1], Sungroh Yoon[1,3,*] and Rhiju Das[2,4,*]

[1]Department of ECE, Seoul National University, Seoul 151-744, Korea, [2]Department of Biochemistry, Stanford University School of Medicine, Stanford, CA 94305, USA, [3]Interdisciplinary Program in Bionformatics, Seoul National University, Seoul 151-744, Korea and [4]Department of Physics, Stanford University, Stanford, CA 94305, USA

*To whom correspondence should be addressed.
Associate Editor: Ivo Hofacker

Received on November 20, 2014; revised on April 27, 2015; accepted on April 29, 2015

Abstract

Motivation: Capillary electrophoresis (CE) is a powerful approach for structural analysis of nucleic acids, with recent high-throughput variants enabling three-dimensional RNA modeling and the discovery of new rules for RNA structure design. Among the steps composing CE analysis, the process of finding each band in an electrophoretic trace and mapping it to a position in the nucleic acid sequence has required significant manual inspection and remains the most time-consuming and error-prone step. The few available tools seeking to automate this band annotation have achieved limited accuracy and have not taken advantage of information across dozens of profiles routinely acquired in high-throughput measurements.

Results: We present a dynamic-programming-based approach to automate band annotation for high-throughput capillary electrophoresis. The approach is uniquely able to define and optimize a robust target function that takes into account multiple CE profiles (sequencing ladders, different chemical probes, different mutants) collected for the RNA. Over a large benchmark of multi-profile datasets for biological RNAs and designed RNAs from the EteRNA project, the method outperforms prior tools (QuSHAPE and FAST) significantly in terms of accuracy compared with gold-standard manual annotations. The amount of computation required is reasonable at a few seconds per dataset. We also introduce an '*E*-score' metric to automatically assess the reliability of the band annotation and show it to be practically useful in flagging uncertainties in band annotation for further inspection.

Availability and implementation: The implementation of the proposed algorithm is included in the HiTRACE software, freely available as an online server and for download at http://hitrace.stanford.edu.

Contact: sryoon@snu.ac.kr or rhiju@stanford.edu

Supplementary information: Supplementary data are available at *Bioinformatics* online.

1 Introduction

RNA molecules play diverse roles in encoding and regulating genetic information, and much of this versatility can be traced to the formation of intricate RNA structures. To this end, chemical probing methodologies provide a general and rapid means to mapping RNA secondary and tertiary structure at single-nucleotide resolution (Weeks, 2010).

There exist many chemical probing techniques, most of which have common experimental procedures, as follows. Given an RNA of interest folded in solution, a chemical reagent modifies the RNA, either cleaving it or forming a covalent adduct with it at a rate correlated with the accessibility of particular moieties at each nucleotide or the frequency at which each nucleotide fluctuates into a conformation activated for chemical reaction. Examples of such chemical reagents, all with distinct mechanisms, include hydroxyl radicals, 2′-OH acylating chemicals (SHAPE), dimethyl sulfate (DMS) and 1-cyclohexyl-3-(2-morpholinoethyl) carbodiimide metho-p-toluenesulfonate (CMCT) (Weeks, 2010). Subsequent reverse transcription detects the modification sites as stops to primer extension at nucleotide resolution. The resulting complementary DNA fragments are resolved in sequencing gels followed by individually quantifying band intensities. Prior to the mid-2000 s, the bottlenecks were the final steps (gel running and band quantification).

To resolve fragments in a more high-throughput fashion, capillary electrophoresis (CE) was developed and is reaching wide use (Mitra *et al.*, 2008). CE-based chemical probing can produce hundreds of electrophoretic profiles exhibiting tens of thousands of individual electrophoretic bands from a single experiment, leading to recent developments in two-dimensional mapping of complex RNA structures (Kladwang *et al.*, 2011) and their excited states (Tian *et al.*, 2014) and extension to large complexes such as entire viruses (Watts *et al.*, 2009) and to RNA design problems (Lee *et al.*, 2014). Further developments in next-generation sequencing readouts are promising but still show biases compared with CE measurements (Kladwang *et al.*, 2014; Lucks *et al.*, 2011).

Analyzing a large number of electrophoretic traces from a high-throughput structure-mapping experiment is time consuming and poses a significant informatic challenge, requiring a set of robust signal-processing algorithms for accurate quantification of the bands embedded in these traces. Software methods for CE analysis include capillary automated footprinting analysis (CAFA; Mitra *et al.*, 2008), ShapeFinder (Vasa *et al.*, 2008), high-throughput robust analysis for CE (HiTRACE; Yoon *et al.*, 2011), fast analysis of SHAPE traces (FAST; Pang *et al.*, 2011) and QuShape (Karabiber *et al.*, 2013).

A typical high-throughput CE analysis pipeline consists of the following steps (Karabiber *et al.*, 2013; Kladwang *et al.*, 2014; Yoon *et al.*, 2011): preprocessing such as normalization and baseline adjustment, alignment, peak detection, band annotation and peak fitting. Among these, band annotation refers to the process of mapping each band in an electrophoretic trace to a position in the nucleic acid sequence. For verification, visual inspection in this phase is inevitable to some extent. However, in practice, this band annotation step often takes significant manual efforts in CAFA and SHAPEfinder, for they were designed to focus more on alignment and peak fitting. HiTRACE, QuShape and FAST have provided improved levels of band annotation support, but band annotation remains still the most time-consuming and error-prone step for large datasets.

This article describes a dynamic-programming based approach to automated band annotation for large CE datasets. These datasets involve at least four and up to hundreds of multiple traces that are aligned for each RNA, based on sequencing ladders for the four different nucleotide types, different chemical modifiers, and/or chemical modification under different solution conditions or with different mutations. The central innovations herein are (i) an accurate and well-tested procedure to integrate information across these multiple traces into a single consensus band annotation with accuracy approaching that of manual annotation and (ii) a reliability estimator for this procedure. Figure 1 shows the overview of the proposed methodology.

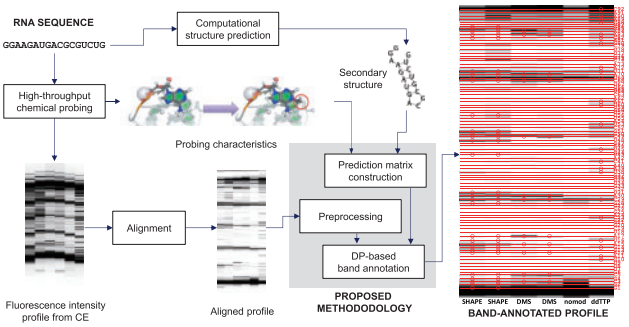

Fig. 1. Overview of the proposed dynamic-programming-based band annotation methodology. Given an RNA sequence, we carry out high-throughput structure-mapping experiments, producing a number of CE traces. If available or estimated through computational prediction, we also provide the RNA's secondary structure. From this information and the characteristics of the chemical probing method used, we derive a prediction matrix that stores expected interaction patterns across the residues and traces. On the basis of the aligned CE traces and prediction matrix, we apply a dynamic-programming approach that finds the optimal selection of the band locations under a well-defined scoring scheme

2 Methods

2.1 Problem definition

Given an RNA sequence $\mathbf{s}$ probed at N nucleotides, assume that we carry out the chemical structure probing of this sequence using M different treatments, each of which is run in a separate capillary lane. Assume that the fluorescence intensity of each capillary is measured over K time points. We define a *profile* (also called a *trace*) as the sequence of intensity values from a capillary. For any particular profile, the reactivity of each nucleotide to the chemical reagent is represented at a specific location in the series of intensity values, and N such locations are sequentially spread throughout the entire profile. All profiles are assumed to be well aligned using the procedure described in Yoon *et al.* (2011), such that each nucleotide corresponds to the same location across all profiles. The entire CE measurement can then be arranged in a $K \times M$ matrix $\mathbf{D}$. Normally, $N \ll K$, i.e. each electrophoretic profile is finely sampled in time. On the basis of the characteristic of the chemical agent used in each treatment and the secondary structure computationally inferred from the input sequence, we can predict the fluorescence intensity at each position of $\mathbf{s}$ for each of M treatments. This prediction can be arranged in an $N \times M$ matrix $\mathbf{P}$ called the *prediction matrix* (see below).

The problem of band annotation is therefore formulated as selecting N out of the K rows of $\mathbf{D}$ using the information in $\mathbf{P}$ in such a way that a certain objective is optimized over all possible $\binom{K}{N}$ possibilities. The selected N points map to the locations of the nucleotides of the sequence $\mathbf{s}$ in the CE measurement (see Supplementary Fig. S1).

The input of the proposed method consists of the following:

- $\mathbf{D} \in \mathbb{R}^{K \times M}$: the fluorescence intensity matrix
- $\mathbf{P} \in \{0,1\}^{N \times M}$: the prediction matrix
- $\mathbf{s} \in \{\mathtt{A}, \mathtt{C}, \mathtt{G}, \mathtt{U}\}^{N}$: the nucleotide sequence

and the output is an array $\mathbf{y} \in \mathbb{Z}_{+}^{N}$ representing N band locations selected out of K.

2.2 Prediction matrix construction

Figure 2a defines the expected reactivity of each type of nucleotide to chemical reagents used for chemical probing under the (un)paired condition. The value of 1 means that the nucleotide is reactive to the reagent, whereas 0 indicates no reactivity. For instance, the DMS chemical modifies A and C but not U and G, and the entries for A and C are one, while those for U and G are zero. We allow the use of numerous chemical probing strategies: DMS alkylation, CMCT and 'others' that can produce bands at all locations, including 2′-OH acylation (the SHAPE strategy) (Kladwang *et al.*, 2014). We also allow input of a secondary structure in dot-parentheses notation. Nucleotides forming base pairs are not expected to show bands in DMS, CMCT, SHAPE and other structure mapping profiles. Sequencing experiments that terminate reverse transcription of the RNA with ddNTP incorporation produce bands after nucleotides complementary to the terminating nucleotide. On the basis of this information, we construct the prediction matrix **P** that stores the expected chemical reactivity for individual residues. The element $p_{ij} \in \mathbf{P}$ indicates such reactivity information of residue i to reagent j.

Figure 2b shows an example RNA sequence with its secondary structure. Figure 2c shows the corresponding prediction matrix **P**.

A

SHAPE			DMS			CMCT			ddTTP		
unpaired	A	1	unpaired	A	1	unpaired	A	0	paired or unpaired	A[a]	1
	U	1		U	0		U	1		U	0
	G	1		G	0		G	1		G	0
	C	1		C	1		C	0		C	0
paired	Any	0	paired	Any	0	paired	Any	0			

B

GGAAGAUGACGCGUCUG

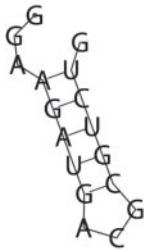

C

Sequence		SHAPE	DMS	CMCT	nomod	ddTTP
order	nt					
1	G	1	0	1	0	0
2	G	1	0	1	0	1
3	A	1	1	0	0	1
4	A	0	0	0	0	0
5	G	0	0	0	0	1
6	A	0	0	0	0	0
7	U	0	0	0	0	0
8	G	0	0	0	0	1
9	A	1	1	0	0	0
10	C	1	1	0	0	0
11	G	1	0	1	0	0
12	C	0	0	0	0	0
13	G	0	0	0	0	0
14	U	0	0	0	0	0
15	C	0	0	0	0	0
16	U	0	0	0	0	0
17	G	1	0	1	0	0

Fig. 2. Prediction matrix. (**A**) Definition of the values appearing in the peak prediction matrix; 1 means that a band is expected in that residue position, whereas 0 means that no band is expected. [a]The bands on ddTTP are expected to be at positions right before where As are located (and showing up immediately afterward in electropherograms of complementary DNA). (**B**) Example target sequence and its estimated secondary structure, here predicted by the Vienna RNA package (Hofacker, 2003). (**C**) The prediction matrix for the example in (**B**)

2.3 Initialization of candidate peaks from profiles

The first step is to locate prominent peaks on each profile (each column of **D**). Peaks in CE profiles are the locations where significant reactivities are observed, implying that bands are more likely to exist at the same position. Thus, these peaks are matched with bands afterward. (Here and below, 'peak' refers to a local maximum in each profile, of which there may be many; whereas 'bands' refers to the desired N band locations.) Let $\mathbf{d}_j$ be the jth column vector of $\mathbf{D}, 1 \le j \le M$. Briefly, the following procedure is executed.

1. Select candidates for the peaks in $\mathbf{d}_j$ that can be mapped into elements of the sequence **s**. These peaks are selected to satisfy the following conditions. First, a peak $\mathbf{d}_j(k)$ must have a higher intensity (a fundamental property of a peak) than those of its neighbors, $\mathbf{d}_j(k-1)$ and $\mathbf{d}_j(k+1)$. Second, a peak must be with a significant curvature which can be measured by the second derivative of time series; since the time series given are discrete, the curvature is estimated as below:

$$\Gamma = \Delta^{-} - \Delta^{+} \tag{1}$$

where

$$\Delta^{-} = \max(\mathbf{d}_j(k) - \mathbf{d}_j(k-1), \frac{(\mathbf{d}_j(k) - \mathbf{d}_j(k-2))}{2})$$

$$\Delta^{+} = \min(\mathbf{d}_j(k+1) - \mathbf{d}_j(k), \frac{(\mathbf{d}_j(k+2) - \mathbf{d}_j(k))}{2})$$

The Δ^{-} and Δ^{+} in (1) approximate the slope of left and right side of peak, respectively, and Γ is the difference between them; thus, the magnitude of Γ represents how abruptly the curve has turned from upward to downward. Now we choose N_j^{peak} peaks with highest Γ from the points satisfying the first condition, where N_j^{peak} is set to twice the number of nucleotides reactive to the chemical agent used for the jth profile (i.e. the number of ones on the jth column of **P**). Call these candidate peak locations A_j^i $(1 \le i \le N_j^{\text{peak}})$.

2. In preparation for the sampling scheme and score function computation below, estimate the ideal separation between bands based on the remaining peak locations: $\rho \triangleq (\min_j k_j^r - \min_j k_j^f)/(N-1)$, where k_j^f and k_j^r are the locations of the foremost peak and the rearmost peak respectively on the jth profile.
3. In preparation for the score function computation below, construct a matrix based on these candidate peak locations called the *bonus matrix* $\mathbf{B} \in \mathbb{Z}^{K \times M}$. Let $\overline{\Gamma}$ be the mean value of Γ_i of the candidate peaks. Initialize **B** to all zero. At each peak A_j^i, we apply a uniform bonus, supplemented by a stronger bonus at sharp peaks: $\mathbf{B}(A_j^i, j) = \overline{\Gamma}/2 + \Gamma_i$.

2.4 Formulation as dynamic programming

2.4.1 Basic motivation

In essence, the band annotation problem is to select N out of K points and match them to peak locations (if at all possible) in an optimal way. This is similar to the problem of aligning two sequences $(1, 2, \ldots, N)$ and $(1, 2, \ldots, K)$ without allowing gaps for the latter.

```
RNA sequence index : -1--2---3...N...-
 Measurement index : 123456789..... ....K
```

In the example above, the first three bands are located at 2, 5 and 9 time units. To find the most probable one among all such alignments, each possible alignment is given a score that represents its likelihood. Dynamic programming can be utilized to find the

solution set with the highest score, which in turn leads to the most likely locations of bands. More formally, define a matrix $\mathbf{F}$ indexed by n and k ($1 \le n \le N$; $1 \le k \le K$) where the value $\mathbf{F}(n,k)$ indicates the maximum score up to the band n and position k. (More details on $\mathbf{F}$ are given below.) The matrix $\mathbf{F}$ is filled up recursively:

$$\mathbf{F}(n,k) = \max_{k-2.5\rho \le k' < k} \{\mathbf{F}(n-1,k') + S(n,k',k)\} \qquad (2)$$

where $S(n,k',k)$ is the score attained by going from position k' to k for band n. As shown in Equation (2), the mappings in $\mathbf{F}(n,k)$ consists of mapping band n to location k added to the solution for $\mathbf{F}(n-1,k^*)$, where k^* is the argmax in (2). The constraint on k' in (2) implies that a jump from k' to k is forward and its width is capped by a reasonable upper bound so that the entire search space can be narrowed down for efficient implementation; it was also confirmed through tests that the existence of upper bound does not affect the outcome.

2.4.2 Degeneracy breaking and primary profile

In the proposed method, a band is allowed to be matched to a candidate peak even if their positions are slightly off from each other; in other words, an exact positional coincidence is not required for a peak-band matching (see Section 2.5.2 for detail). Thus, the formalization of our problem in the previous section allows for an undesired scenario in which two different bands will be matched to the same closest peak (see Supplementary Fig. S2); this can be problematic especially near strong peaks [high Γ in (1)]. To avoid such degeneracies, an additional search variable p is introduced: the relative position of the matched peak to the band position k. The tuple (n, k, p) corresponds to the instance in which the band n is located at position k and matched with the peak at $k+p$ if there is any; there is no score bonus if there is no peak at the position. The matrix $\mathbf{F}$ is now redefined as a 3-dimensional matrix as follows:

$$\mathbf{F}(n,k,p) = \max_{\substack{k-2.5\rho \le k' < k \\ |p| < \rho/2 \\ k'+p' < k+p}} \{\mathbf{F}(n-1,k',p') + S(n,k',k,p)\} \qquad (3)$$

The constraint $|p| < \rho/2$ is to restrict bands to be matched only with nearby peaks, and the last constraint $k'+p' < k+p$ means that two distinct bands cannot share the same peak. One problem that arises with the use of p is that there should be M such p's for M profiles, implying that the matrix $\mathbf{F}$ should not be three-dimensional but actually $(M+2)$ dimensional. However, this would make solving this problem too costly. As a compromise, the problem is simplified by choosing one primary profile among M profiles so that p is applied only to it; therefore, $\mathbf{F}$ may remain as a three-dimensional matrix. Our software automatically determines the primary profile based on the data type with a preference for sequencing ladders. For our datasets, the last profile (a ddTTP ladder) was selected; without loss of generality, $\mathbf{d}_M$ will be considered as the primary profile in the rest of this article.

2.4.3 Backtracking

The backtracking matrices $\mathbf{L}_k$, $\mathbf{L}_p$ for finding the solution itself are given by

$$\begin{aligned}\mathbf{L}(n,k,p) &= (\mathbf{L}_k(n,k,p), \mathbf{L}_p(n,k,p)) \\ &= \operatorname*{argmax}_{\substack{k-2.5\rho \le k' < k \\ |p| < \rho/2 \\ k'+p' < k+p}} \{\mathbf{F}(n-1,k',p') + S(n,k',k,p)\}\end{aligned} \qquad (4)$$

and, respectively, store the position k' and the relative peak location p' from which $\mathbf{F}(n,k,p)$ is derived as in (3). The output array $\mathbf{y}$ is derived from $\mathbf{L}_k$ and $\mathbf{L}_p$ as follows:

$$\begin{aligned}\mathbf{y}(n) &= (\mathbf{y}_k(n), \mathbf{y}_p(n)) \\ &= \begin{cases} \operatorname*{argmax}_{k,p} \{\mathbf{F}(N,k,p)\}, & \text{if } n = N; \\ \mathbf{L}(n+1, \mathbf{y}_k(n+1), \mathbf{y}_p(n+1)), & 1 \le n \le N-1. \end{cases}\end{aligned} \qquad (5)$$

The value of $\mathbf{y}_k(n)$ corresponds to the location of the nth band in the input sequence $\mathbf{s}$. Figure 3 illustrates the proposed dynamic-programming formulation with an example.

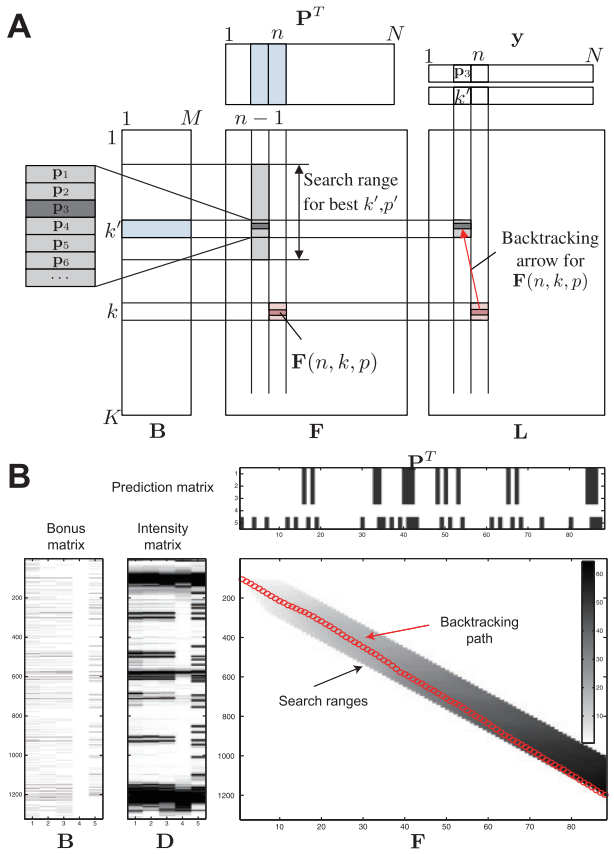

Fig. 3. Formulation as dynamic programming. (**A**) $\mathbf{F}(n,k,p)$ depends on $\mathbf{F}(n-1,k',p')$ in the previous column and the gap bonus $S(n,k',k,p)$ between them. The best tuple (k',p') that maximizes $\mathbf{F}(n,k,p)$ is searched for in the range $k-2.5\rho \le k' < k$; $k'+p' < k+p$ and is stored in the backtracking matrices $\mathbf{L}_k(n,k,p)$, $\mathbf{L}_p(n,k,p)$. The computation of $S(n,k',k,p)$ is based on the bonus matrix $\mathbf{B}$ and the prediction matrix $\mathbf{P}$ (Section 2.5). (**B**) Example. The dataset used is 'FMN Aptamer with single binding site'. $N=88$, $M=5$, $K=1324$. The backtracking path is represented by a series of red circles superimposed on the score matrix $\mathbf{F}$; since $\mathbf{F}$ is 3-dimensional, the figure alternatively represents a reduced matrix $\mathbf{F}'$ defined by $\mathbf{F}'(n,k) = \max_{p'} \mathbf{F}(n,k,p')$. The output array $\mathbf{y}_k$, which stores the position of each circle, indicates the band locations

2.5 Description of score term

The score term in (3) consists of the following two components:

$$S(n,k',k,p) = S_{\text{dist}}(n, k-k') + w_{\text{peak}} \cdot \mathbf{S}_{\text{peak}}(k,p) \cdot \mathbf{P}(n,:) \qquad (6)$$

where S_{dist} and $\mathbf{S}_{\text{peak}}$ are functions returning vectors of nonnegative elements, and $\mathbf{P}(n,:)$ is the nth row of the prediction matrix $\mathbf{P}$. The dot product in the second term is a sum over all lanes m from 1 to M. A coefficient w_{peak} of 1.0 gave acceptable annotations in initial tests and was not further optimized.

2.5.1 Distance bonus term

It is empirically supported that the length between consecutive locations, k' and k, is quite evenly distributed. S_{dist} is the bonus term that utilizes this fact and induces the dynamic programming to end up with regularly stretched output. In addition, observations on reference annotations suggest that a gap between two consecutive locations tends to be shorter when the preceding location corresponds to 'G' in the RNA sequence (Mills and Kramer, 1979; Sasaki *et al.*, 1998). These observations lead to the definition of distance bonus term as follows:

$$S_{\text{dist}}(n,d) = \frac{f_{(\rho',\frac{\rho}{2})}(d)}{f_{(\rho',\frac{\rho}{2})}(\rho')} \tag{7}$$

where

$$\rho' = \begin{cases} \frac{2}{3}\rho, & \text{if} \quad \mathbf{s}(n-1) = \mathtt{G}; \\ \rho, & \text{otherwise} \end{cases}$$

and $f_{(\mu,\sigma)}$ is the density function of $N(\mu,\sigma)$. That is, $S_{\text{dist}}(n,d)$ reaches its maximum value 1 when $d = \rho'$ and decreases along a Gaussian curve as d deviates from ρ'.

2.5.2 Peak bonus term

The second score term favors band locations near peaks of the electrophoretic profiles with a significant curvature. $\mathbf{S}_{\text{peak}}$ is a function that returns a nonnegative M-dimensional value, where each of its entries represents the peak bonus from each profile:

$$\mathbf{S}_{\text{peak}}(k,p) = (S^1_{\text{peak}}(k), \ldots, S^{M-1}_{\text{peak}}(k), S^M_{\text{peak}}(k,p)) \tag{8}$$

where S^m_{peak} stands for the bonus from matching a peak to a band in $\mathbf{d}_m$, assuming such a band exists. The bonus was designed to be boosted for a greater curvature at the peak and the proximity of the peak to the band, so S^m_{peak} is defined as the product of a Gaussian density function and an entry of $\mathbf{B}$ corresponding to the candidate peak closest to location k:

$$S^m_{\text{peak}}(k) = \max_{|q|<\rho/2} \frac{f_{(0,\frac{\rho}{5})}(q)}{f_{(0,\frac{\rho}{5})}(0)} \cdot \mathbf{B}(k+q,m) \tag{9}$$

for $m < M$, and

$$S^M_{\text{peak}}(k,p) = \frac{f_{(0,\frac{\rho}{5})}(p)}{f_{(0,\frac{\rho}{5})}(0)} \cdot \mathbf{B}(k+p,M) \cdot (M-1) \tag{10}$$

As described above, this last term is taken from the primary profile (typically a sequencing ladder) rather than searching for optimal peak/band matches across all profiles to allow degeneracy breaking at reasonable computational expense. [A separate dynamic-programming-based band annotation algorithm was also tested which does not carry out the peak/band degeneracy breaking of Equation (10) and gave slightly worse performance; see Supplementary Fig. S3.] The bonus in (10) is non-zero where $k+p$ coincides with a candidate peak location A^i_M. For some cases, the primary profile might have regions with few candidate peaks, and such matches do not occur; the bonus values become zero and the optimal values of p are instead set by positional constraints in (3) and candidate peaks in other profiles (9). A large number of such failed matches flag an unreliable band annotation, as described next.

2.6 Reliability evaluation

Although the presented band annotation method was found to be quite accurate, it was not perfect. We therefore sought a method to assess the reliability of automatically determined band locations prior to practical application. We devised a score to predict the quality of results. The idea behind the score is that when optimization of Equation (6) fails to achieve the desirable solution, we typically see extraordinarily short or long distances between consecutive locations (little information from S_{dist}) or bands on the primary profile without proper matching to peaks (little information from S^M_{peak}). The E-score is defined with the following terms:

- n_1: number of bands on the primary profile without corresponding peak.
- n_2: number of gaps with length $< \rho/4$ or $> 2\rho$.
- N^{peak}_M: number of bands on the primary profile predicted by $\mathbf{P}$.
- $E = 1 - \max(\frac{n_1}{N^{\text{peak}}_M}, \frac{n_2}{K-1})$

E-score is a value between 0 and 1 and conservatively estimates the fraction of well-annotated bands in the output. The relationship between E-score and accuracy is presented in Section 3.

3 Results

3.1 Robust determination of band positions

Figure 4a–c shows the electrophoretic profiles annotated with band locations by three different methods: reference, proposed and QuShape (Karabiber *et al.*, 2013), respectively. The reference annotation was based on expert assignments carried out at the time of data acquisition (Lee *et al.*, 2014). QuShape was chosen as the comparison target for its superior accuracy in band annotation relative to other software we tested, FAST and ShapeFinder (data not shown); no-modification and ddTTP ladder profiles were used as references (RXS1, BGS1) while running QuShape. Visual inspection suggests that the proposed method produces annotations more compatible with the reference. In this profile, the annotation determined by QuShape deviates from the reference position, particularly near the beginning of sequence.

To generally and quantitatively assess the accuracy of automated band annotation, we applied the proposed method and QuShape to 95 datasets acquired in the EteRNA project (Table 1). For both methods, we computed the mean squared error (MSE) of the band

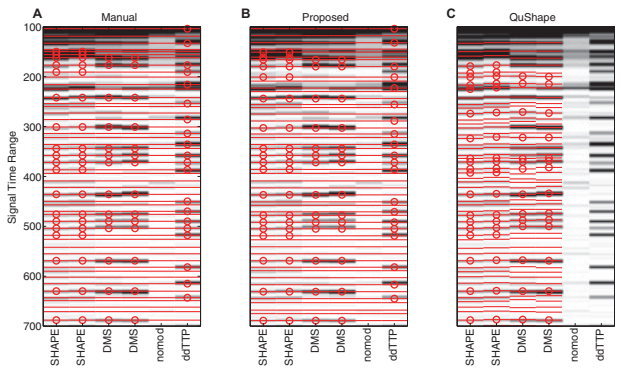

Fig. 4. Determination of band locations for dataset 'ViennaRNA design 03'. (**A**) Reference (manual) annotation. Red horizontal lines represent all determined band locations corresponding to RNA sequence. Red circles represent the bands reactive to chemical agents for each profile. (**B**) The band locations determined by the proposed method. (**C**) The band locations found by QuShape (Karabiber *et al.*, 2013)

Table 1. High-throughput RNA structure mapping datasets analyzed by the proposed method (total 522 profiles and 47 210 bands)

Name	No. profiles	No. nt	No. bands per profile	No. total bands
R45[a]	60	108	88	5280
R46[a]	80	108	88	7040
R47[b]	90	112	92	8280
R47B[b]	36	112	92	3312
R48[b]	96	112	92	8832
R49[b]	18	112	92	1656
R49B[c]	48	115	95	4560
R50[c]	54	115	95	5130
R43[d]	40	98	78	3120

Excluding the last line, there are 95 datasets. More details of these 95 datasets are described in Lee *et al.* (2014). FMN, flavin mononucleotide.

[a]FMN aptamer with single binding site (Lee *et al.*, 2014).

[b]FMN aptamer with single binding site II.

[c]FMN binding branches.

[d]The backward C.

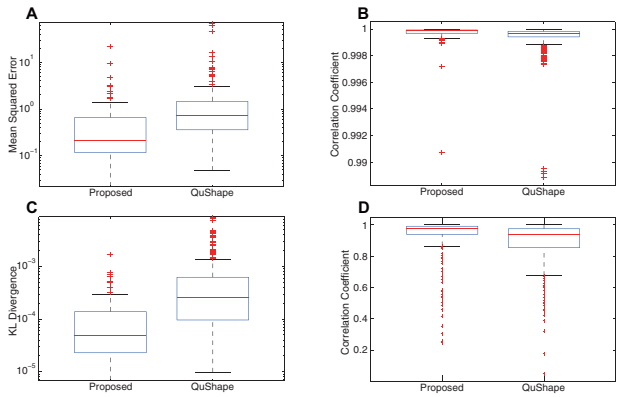

Fig. 5. Proposed method (left) versus QuShape (right). Each plot represents each metric's distribution across 95 datasets. (**A**) MSE for band locations. (**B**) Pearson's correlation coefficient *r* for band locations. (**C**) KL divergence for band locations. (**D**) Pearson's correlation coefficient *r* for area quantification. MSE units are normalized, so that average distance between band locations is unity

locations determined by the proposed method with respect to the reference locations, in units of average distance between locations. For a sense of scale, the typical MSE achieved by expert annotation is 0.15, based on comparisons of different experts' annotations with each other and to next-generation-sequencing-based measurements, where sequence annotation is unambiguous (Kladwang *et al.*, 2014); see Supplementary Figure S4. In our experience, a band annotation result with MSE lower than 0.5 typically requires no or a small number of manual single-click corrections. The box plots in Figure 5a–c and individual MSE values (Supplementary Tables S1 and S2) reveal that the proposed method outperforms QuShape across the datasets. For example, the median MSE of the proposed method is 0.21, well under our target value of 0.5, compared with 0.72 from QuSHAPE. As separate metrics of accuracy, we measured the Pearson's correlation coefficient *r* and the Kullback–Leibler (KL) divergence between the reference and computationally determined band positions. Again, the average correlation coefficient of the proposed method is 1.68 times closer to 1, and the average KL divergence is 5.84 times smaller. These results quantitatively confirm what we observed qualitatively on using these tools: significantly less manual intervention is needed with the proposed method compared with

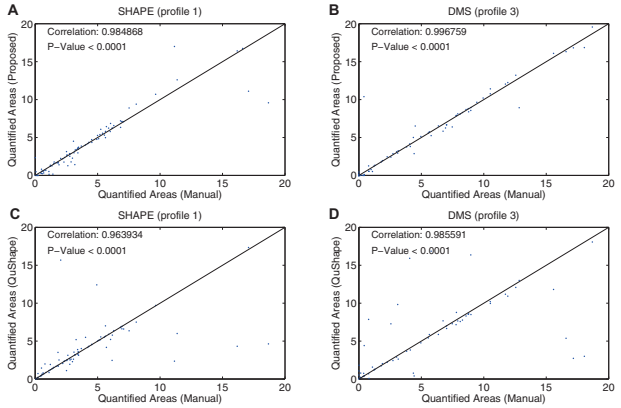

Fig. 6. Accuracy of quantifying peak areas for dataset 'FMN Binding Branches'. (**A**, **B**) Correlation of the reference and the quantified areas by the proposed method is shown for profiles 1 (SHAPE) and 3 (DMS). (**C**, **D**) Correlation of the reference and the areas quantified by QuShape. Displayed correlation values are Pearson's correlation coefficient *r*

QuShape. Further tests confirmed the utility of using multiple profiles, secondary structure information and peak match degeneracy breaking in producing accurate band annotations (Supplementary Fig. S3).

3.2 Accurate peak-area quantification

In the RNA structure mapping pipeline, the band annotation is followed by peak deconvolution, which fits each band with a Gaussian curve and outputs the quantified area of the band. To see how these final band quantification results are impacted by the band annotation method, we calculated Pearson's correlation coefficients between band areas quantified based on the band annotation found by the proposed method and those quantified based on the reference annotation. We also repeated the calculation with the band intensities quantified by QuShape. For fair comparison, we applied the same peak deconvolution software (HiTRACE; Yoon *et al.*, 2011) to these three methods.

As one example, Figure 6a and b shows the correlation of results between the proposed method and reference for a specific dataset (flavin mononucleotide binding branches) for two chemical modification strategies (SHAPE and DMS). Figure 6c and d shows the correlation between the QuShape and reference results, which is visually worse than the proposed method in both cases. Over all the datasets, Figure 5d and Supplementary Table S1 gives the distribution of the Pearson's correlation coefficients. The median correlation coefficient for the proposed method is 0.976, which is higher than that for QuShape (0.939) and the distribution for the proposed method shows smaller variance. This observation suggests that using the proposed band annotation can significantly enhance the accuracy of band quantification.

3.3 *E*-score reliability metric predicts MSE accuracy

In Section 2.6, we proposed *E*-score to evaluate the quality of results from our method. We assessed the use of *E*-score based on its ability to predict the accuracy of the band annotations compared with gold standard annotations, quantitatively evaluated as MSE. Figure 7a shows the distribution of MSE for results satisfying $E = 1.0$; these values are substantially smaller than those in Figure 7b, which includes all 95 datasets. For example, all 26 results under constraint $E = 1.0$ have MSE below 0.5 as shown in Figure 7a, confirming that a

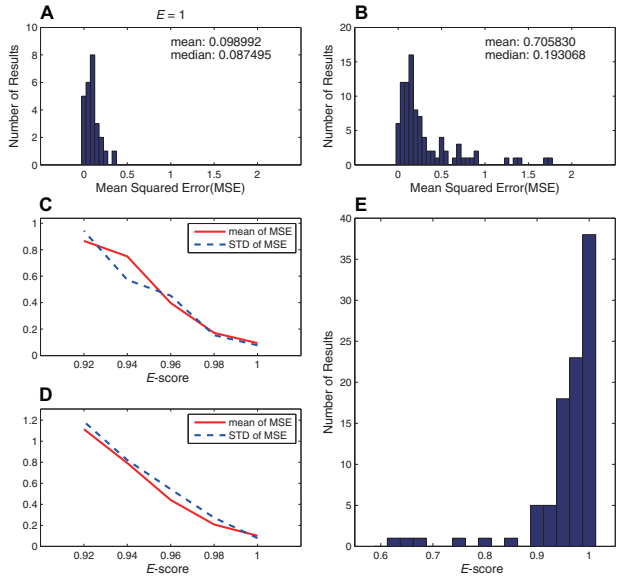

Fig. 7. (**A**) Distribution of MSE for the results with 1 *E*-score. (**B**) Distribution of MSE for the whole 95 results (five results with MSE > 2 are omitted for better demonstration). (**C**) Trends of mean and standard deviation of MSE with respect to *E*-score over artificial data generated from a single original dataset. (**D**) Trends of mean and standard deviation of MSE with respect to *E*-score for artificial data generated from the whole 95 datasets. (**E**) Distribution of *E*-score over 95 datasets

'perfect' *E*-score essentially guarantees high quality of band annotations; furthermore, 50 out of 51 results with $E > 0.97$ have MSE below 0.5 (even the one exception has MSE < 1). In addition to this experimental test, artificial datasets were generated based on the original datasets through random convolution in terms of amplitude and interval for further verification. Figure 7c and d show the trends of mean and standard deviation of MSE with respect to *E*-score, where Figure 7c comes from artificial data generated from a single dataset, whereas artificial data involved in Figure 7d was generated from all 95 datasets. The trends shown in Figure 7c and d further confirm that a lower *E*-score corresponds to MSE values with higher (worse) mean and standard deviation. Figure 7e shows the histogram of the *E*-scores over the 95 datasets prepared. Overall, 39% of the datasets have *E*-score equal to 1, and 84% have *E*-score greater than 0.97, suggesting that poor *E*-scores and subsequent detail manual correction will be encountered in a minority of cases.

3.4 Results in longer, biological RNA sequences

In an effort to test the proposed method's compatibility with a wide array of high-throughput RNA structure mapping datasets, we prepared sample experimental datasets of biologically derived RNAs. These additional 21 datasets include a class I ligase (Bagby *et al.*, 2009), the Tetrahymena L-21 ScaI group I ribozyme (Russell *et al.*, 2006), a four-way junction from the *Escherichia coli* 16S ribosomal RNA (Tian *et al.*, 2014), RNA replicases (C19, tC19 and tC19Z) (Wochner *et al.*, 2011), human Hox transcripts 5′ UTR (Hox5 and Hox9D189) (Xue *et al.*, 2015) and RNA Puzzle entries (#5–10 and 12) (Cruz *et al.*, 2012). In each dataset, complete sets of chemical modifier reactions (no modification, SHAPE, DMS, CMCT) and reference ladders (ddNTPs) are present. In addition, a hepatitis delta virus genomic segment studied previously allowed direct comparison to the FAST software (Supplementary Fig. S5) (Pang *et al.*, 2011). These RNAs had lengths up to 400 nucleotides, significantly longer than the 100-nt EteRNA designs (Table 1). Despite this increase in length, the band annotation results from the proposed method were still consistent with the reference expert annotation. Excluding an abnormal result from the Tetrahymena ribozyme caused by an experimental issue that disallowed alignment of sequencing ladders, the maximum of MSE is only 0.68. Furthermore, the two worst MSE values (0.68 and 0.63) and two lowest *E*-scores (0.83 and 0.90) coincide in the results for RNA puzzle 6 (an adenosylcobalamin riboswitch) and tRNA(phe), confirming *E*-score's utility.

4 Discussion

The proposed method for band annotation is unique in its ability to take into account all available CE profiles; prior methods (such as those available in QuShape and FAST) have focused on a single profile at a time with a reference profile if needed. The distinctive robustness of the proposed method is primarily attributed to this capability to integrate information across profiles. The method does require an accurate alignment of all profiles prior to band annotation. Our prior work (Yoon *et al.*, 2011) described a different dynamic programming algorithm to accomplish this preceding alignment based on standards co-loaded with each sample. In well over 100 datasets analyzed here, we saw only one case where inter-profile alignment was problematic (Tetrahymena ribozyme) and required manual intervention. Therefore, our alignment and annotation results herein confirm that all steps, including alignment and annotation, of RNA structure mapping CE analysis can now be routinely achieved through automated algorithms.

To flag cases with uncertain automated band annotation, we have introduced the *E*-score for reliability estimation. According to our results, given any dataset for CE analysis, the band annotations with $E > 0.97$ are almost always reliable and can be safely adopted for final steps of band quantitation, whereas the results with $E \leq 0.97$ are less likely to reliable. Informally, we have encountered datasets in which even expert annotation is ambiguous and has required special additional experiments (such as co-loading sequencing ladders in the same color as the sample) to resolve (Tian *et al.*, 2014). This suggests that automated band annotation cannot improve much further; a valuable development would be reliability estimates for specific subsets of bands rather than a global number. An additional useful development would be use of known band intensities based on prior experiments (Karabiber *et al.*, 2013) or on base pair probability estimates, rather than coarse predictions for profiles based on sequence, modifier and a single secondary structure.

The proposed algorithm has order of *NK* time and space complexity, and the practical time demand of band annotation was reasonable in our experiments. The proposed method was implemented in the MATLAB programming environment (The MathWorks, http://www.mathworks.com), and under the experimental setup used (sequential execution on a Intel core i5 4570 processor with 8-GB main memory), the total time demand of annotating bands in all the 95 datasets did not exceed 4 min (for each dataset, mean 2.2837 s; median 2.2707 s).

5 Conclusion

In the analysis of CE profiles, band annotation has remained the most time-consuming and error-prone step, due to the lack of robust computational tools for automating the process. Using a dynamic-programming approach, the proposed algorithm can find an optimal arrangement of bands in a given CE profile, under a scoring scheme

suitable for high-throughput CE experiments with multiple profiles. On over 100 CE datasets including designed and biological RNAs, the proposed method identified the band positions matching the reference positions with accuracy sufficiently high as to obviate or significantly reduce manual correction. Finally, the quality of the band positions are well predicted by *E*-score, flagging unreliable annotations to the user.

Acknowledgement

The authors thank Menashe Elazar at the Glenn Laboratory at Stanford University for providing the HDV ribozyme data.

Funding

This work was supported in part by the National Research Foundation of Korea funded by the Ministry of Education, Science and Technology (grant no. 2011-0009963 and no. 2014M3C9A3063541 to S.Y.) and in part by a Burroughs-Wellcome Foundation Career Award at the Scientific Interface and the U.S. National Institutes of Health (NIGMS R01GM100953 to R.D. for computational work).

Conflict of Interest: none declared.

References

Bagby,S.C. *et al.* (2009) A class I ligase ribozyme with reduced Mg^{2+} dependence: selection, sequence analysis, and identification of functional tertiary interactions. *RNA*, **15**, 2129–2146.

Cruz,J.A. *et al.* (2012) RNA-puzzles: a CASP-like evaluation of RNA three-dimensional structure prediction. *RNA*, **18**, 610–625.

Hofacker,I. (2003) Vienna RNA secondary structure server. *Nucleic Acids Res.*, **31**, 3429–3431.

Karabiber,F. *et al.* (2013) Qushape: rapid, accurate, and best-practices quantification of nucleic acid probing information, resolved by capillary electrophoresis. *RNA*, **19**, 63–73.

Kladwang,W. *et al.* (2011) A two-dimensional mutate-and-map strategy for non-coding RNA structure. *Nat. Chem.*, **3**, 954–962.

Kladwang,W. *et al.* (2014) Standardization of RNA chemical mapping experiments. *Biochemistry*, **53**, 3063–3065.

Lee,J. *et al.* (2014) RNA design rules from a massive open laboratory. *Proc. Natl. Acad. Sci. USA*, **111**, 2122–2127.

Lucks,J.B. *et al.* (2011) Multiplexed RNA structure characterization with selective 2-hydroxyl acylation analyzed by primer extension sequencing (shape-seq). *Proc. Natl. Acad. Sci. USA*, **108**, 11063–11068.

Mills,D.R. and Kramer,F.R. (1979) Structure-independent nucleotide sequence analysis. *Proc. Natl. Acad. Sci. USA*, **76**, 2232–2235.

Mitra,S. *et al.* (2008) High-throughput single-nucleotide structural mapping by capillary automated footprinting analysis. *Nucleic Acids Res.*, **36**, e63.

Pang,P.S. *et al.* (2011) Simplified RNA secondary structure mapping by automation of SHAPE data analysis. *Nucleic Acids Res.*, **39**, e151.

Russell,R. *et al.* (2006) The paradoxical behavior of a highly structured misfolded intermediate in RNA folding. *J. Mol. Biol.*, **363**, 531–544.

Sasaki,N. *et al.* (1998) Identification of stable RNA hairpins causing band compression in transcriptional sequencing and their elimination by use of inosine triphosphate. *Gene*, **222**, 17–24.

Tian,S. *et al.* (2014) High-throughput mutate-map-rescue evaluates shape-directed RNA structure and uncovers excited states. *RNA*, **20**, 1815–1826.

Vasa,S. *et al.* (2008) ShapeFinder: a software system for high-throughput quantitative analysis of nucleic acid reactivity information resolved by capillary electrophoresis. *RNA*, **14**, 1979–1990.

Watts,J.M. *et al.* (2009) Architecture and secondary structure of an entire HIV-1 RNA genome. *Nature*, **460**, 711–716.

Weeks,K. (2010) Advances in RNA structure analysis by chemical probing. *Curr. Opin Struct. Biol.*, **20**, 295–304.

Wochner,A. *et al.* (2011) Ribozyme-catalyzed transcription of an active ribozyme. *Science*, **332**, 209–212.

Xue,S. *et al.* (2015) RNA regulons in Hox 5′ UTRs confer ribosome specificity to gene regulation. *Nature*, **517**, 33–38.

Yoon,S. *et al.* (2011) HiTRACE: high-throughput robust analysis for capillary electrophoresis. *Bioinformatics*, **27**, 1798–1805.